Journal of Physics: Conference Series

Effect of oxygenation process on flux pinning in pristine and $BaHfO_3$ nanocomposite $GdBa_2Cu_3O_7$ superconducting thin films

Journal of Physics: Conference Series **1559** (2020) 012038 doi:10.1088/1742-6596/1559/1/012038

Effect of oxygenation process on flux pinning in pristine and $BaHfO_3$ nanocomposite $GdBa_2Cu_3O_7$ superconducting thin films

Ruslan Popov[1], Kai Ackermann[1], H. Rijckaert[2], Jens Hänisch[1], I. Van Driessche[2], Bernhard Holzapfel[1]

[1]Karlsruhe Institute of Technology, Institute for Technical Physics, Hermann-von-Helmholtz-Platz 1, 76344, Eggenstein-Leopoldshafen, Germany
[2]SCRiPTS, Department of Chemistry, Ghent University, Krijgslaan 281-S3, 9000 Ghent, Belgium

E-mail: ruslan.popov@kit.edu

Abstract. Pristine and $BaHfO_3$ (BHO) nanocomposite $GdBa_2Cu_3O_7$ (GdBCO) superconducting thin films were deposited at 800 °C, 0.4 mbar O_2 partial pressure using a Nd:YAG laser (λ =355 nm) with 10 Hz frequency on MgO substrate. The influence of the oxygenation process on flux pinning and electrical transport properties was investigated by changing the annealing temperature (T_{ann}) between 450 °C and 780 °C and the holding time (t_{hold}) between 10 and 30 min. The irreversibility field shows the largest shift toward higher fields for T_{ann} = 450 °C and thus the largest in-field J_c. Angular dependence of J_c for most of the pristine GdBCO films exhibits a large peak for $B\|c$, however the sample with T_{ann} = 550 °C has a large peak in the 90°-120° region, i.e. near $B\|ab$. For BHO nanocomposites, a decrease in T_{ann} increases in-field J_c by a factor of 2.

1. Introduction

$RE$$Ba_2Cu_3O_{7-\delta}$ (RE-rare earth, REBCO) based superconductors were thoroughly investigated during last decades due to possible applications in superconducting motors, fault current limiters, generators and superconducting electronics. REBCO superconducting thin films have relatively high critical temperatures (T_c), which allows operation at liquid nitrogen temperatures and in addition high critical current density (J_c). One of the advantages of REBCO thin films is the presence of growth-related defects and artificial pinning centers (APCs), which results in high in-field J_c values due to the interaction of flux lines with structural defects. In the seminal work of J. L. MacManus-Driscoll *et al.* [1] on the example of $YBa_2Cu_3O_7$ (YBCO) thin films containing $BaZrO_3$ (BZO) nanoparticles 1.5-5 fold improvement of in-field J_c by introduction of secondary phases has been demonstrated. Additionally, as it was shown in the studies of A. Goyal *et al.* [2] and Y. Yamada *et al.* [3] on YBCO films with BZO or yttria-stabilized zirconia nanocomposites that secondary phases can form columnar-like defects in the YBCO matrix. Regardless of many studies on the influence of deposition parameters, such as substrate temperature (T_{sub}), laser repetition rate (f), oxygen partial pressure (p_{O_2}) and laser energy density [4–9], post-annealing treatment of such thin films with APCs has not been studied widely. During deposition, the insulator $RE$$Ba_2Cu_3O_6$ tetragonal phase is formed and an oxygenation procedure is necessary to

induce additional oxygen to form CuO chains of orthorombic phase, which are essential for the superconductivity [10, 11]. Moreover, T_c and self-field as well as in-field J_c strongly dependent on the oxygen content, and thus can affect both self-field and in-field J_c values. Recent studies of J. W. Lee *et al.* [12] and W. J. Oh *et al.* [13] on oxygenation of $GdBa_2Cu_3O_7$ (GdBCO) coated conductors (CCs) showed that different oxygen pressures and holding times (t_{hold}) can lead to a reduction of stacking faults density and increase in in-field J_c. Regardless of huge amounts of research and publication in the field of superconducting *RE*BCO thin films influence of the oxygenation process in (PLD-grown) *RE*BCO films with APCs is still not clarified. Therefore, we studied the influence of the annealing temperature (T_{ann}) on transport and pinning properties in superconducting GdBCO and GdBCO+2.5wt% $BaHfO_3$ (BHO) thin films.

2. Experimental methods

Thin films were deposited using 3rd harmonic ($\lambda = 355$ nm) Nd:YAG laser on MgO (100) single crystals from pristine GdBCO and mixed GdBCO+2.5wt% BHO targets. The laser beam was focused by a lens into the spot of 2 mm diameter, resulting in a laser energy density of 2.5 J/cm^2. For each sample 6000 pulses were used to achieve films thickness of 200 - 250 nm. For both systems, T_{sub} = 800 °C, f = 10 Hz, p_{O_2} = 40 Pa is found to be an optimum [9]. After depositon, all samples were cooled down to T_{ann} between 450 °C and 780 °C, with further input of O_2 up to 400 mbar, kept at T_{ann} for 10-30 min (holding time, t_{hold}) and cooled to room temperature. t_{hold} was increased from 10 to 30 min for lower T_{ann} due to lower diffusion rates of oxygen into GdBCO matrix [14, 15]. To check the phase purity and microstructure films were investigated by x-ray diffraction (XRD) on a Bruker D8 diffractometer with Cu K_α radiation. Transition temperatures were determined with a criterion 10% of the normal state resistance from resistivity measurements. Afterwards, microbridges of 1 mm length and 20-30 µm width were prepared by photolithography and wet-chemical etching for transport measurement in four-point geometry. Quantum design PPMS with magnetic field up to 14 T used for transport measurements at different temperatures, magnetic fields and field orientation in maximum Lorentz force configuration. 1 µV/cm electrical field was used as criterion for J_c and $R(T)/R(100K) \approx 10^{-7}$ criterion for the irreversibility temperatures. Bright-Field (BF) scanning transmission electron microscope (STEM) was conducted using a Cs-corrected JEOL JEM 2200FS device, operated at 200 kV. Samples for BF-STEM were prepared by cutting a cross-sectional lamella via the Focused Ion Beam (FIB) technique in a FEI Nova 600 Nanolab Dual Beam FIB-SEM. The lamella were extracted using the *in-situ* lift out procedure with an Omniprobe extraction needle [16].

3. Results and Discussion

3.1. Influence of oxygenation on flux pinning in pristine GdBCO thin films

As it can be seen from Table 1, all GdBCO films have similar T_c values around 92.7 K. The *c*-axis lattice parameter slightly increases with decrease of T_{ann} and reaches it maximum at 450 °C and t_{hold} = 30 min, which means the oxygen content goes from overdoped region around c = 1.1726 nm to an optimally doped with c = 1.1732 nm. In addition *c*-axis lattice parameters correspond well to other studies on *RE*BCO thin films [17, 18]. Regardless of T_c, self-field J_c for pristine samples range from 1.2 to 4.7 MA/cm^2 and is in good agreement with other works on pristine GdBCO growth on single crystals [19, 20]. 4.7 MA/cm^2 is achieved for the sample annealed at 650 °C and t_{hold} = 30 mim. However, the highest pinning force density of 6.2 GN/m^3 at 77 K is achieved at T_{ann} = 450 °C. All pristine GdBCO thin films with T_{ann} = 450 °C-780 °C and t_{hold} = 10-30 min show strong GdBCO (00l) peaks in θ-2θ XRD scans, Fig. 1, which indicates highly *c*-axis oriented growth. Only the sample at T_{ann} = 700 °C and t_{hold} = 20 min shows (h00) peaks from *ab*-grains. Cross-sectional BF-STEM images for T_{ann} = 780 °C (Fig. 2 A-B) and for T_{ann} = 550 °C (Fig. 2 C-D) reveal stacking faults and threading dislocations. In contrast to

Table 1: Basic properties of pristine and 2.5wt% BHO GdBCO thin films

T_{ann}, °C pristine	T_{ann}, °C BHO	t_{hold}, min	T_c, K	c, nm	$J_c(0)$ at 77K, MA/cm^2	$F_{p,max}$(77 K), GN/m^3
780		10	92.1	1.1726	2.7	2.7
700		20	92.3	1.1726	1.3	2.5
650		30	92.7	1.1726	4.7	5.8
550		30	92.7	1.1728	2.2	3.6
450		30	92.8	1.1732	4.2	6.2
	780	10	90.5	1.1756	1.2	4.9
	700	20	91.1	1.1749	2	11.9
	550	30	90.9	1.1750	1.8	11.4

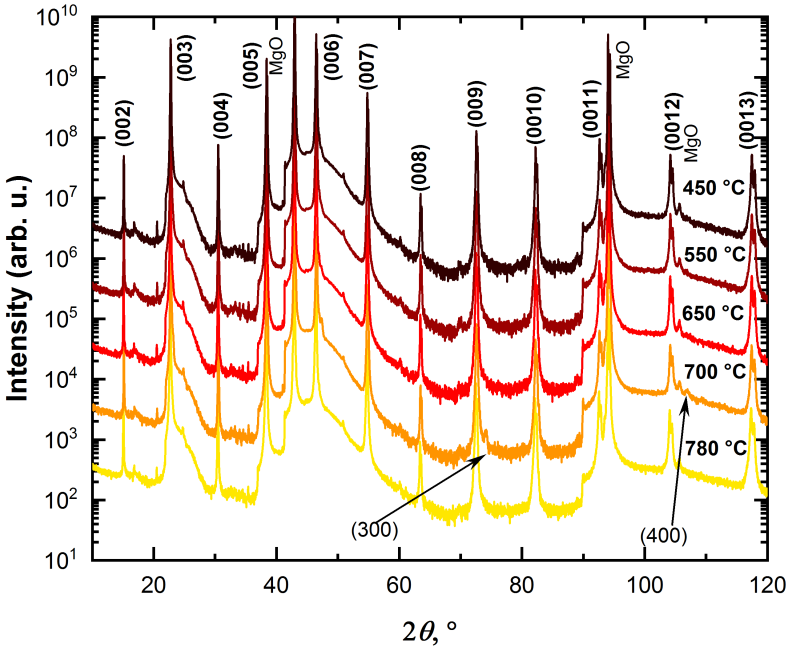

Figure 1: $\theta - 2\theta$ scan of PLD-grown pristine GdBCO films on MgO substrate annealed at 450 °C-780 °C and t_{hold} = 10-30 min. All samples have GdBCO (00l) peaks. T_{ann} = 700 °C has (h00) peaks from ab-grains.

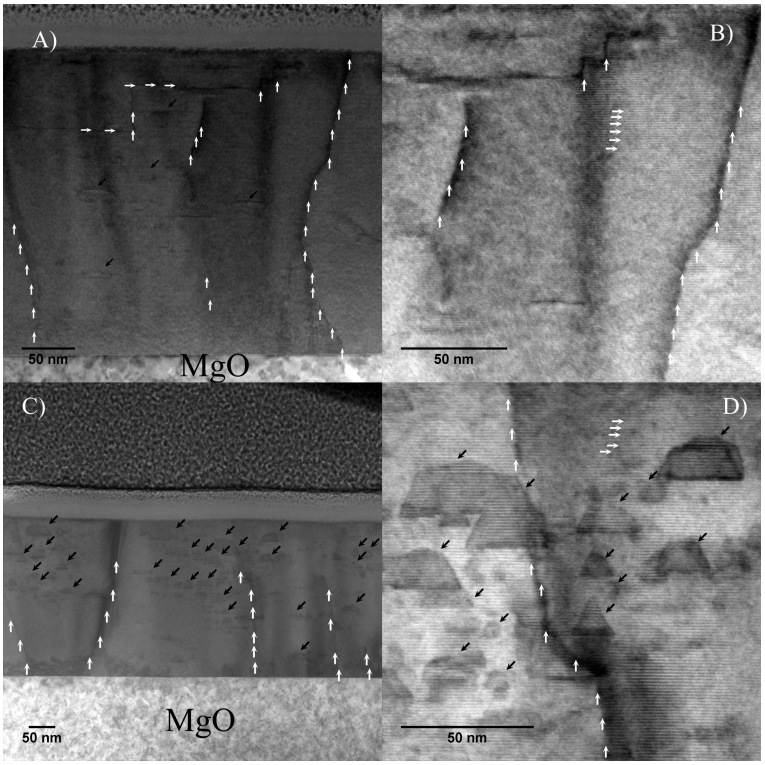

Figure 2: Cross-sectional BF-STEM images of PLD-grown pristine GdBCO films on MgO substrate annealed at 780 °C (A-B) and 550 °C (C-D). White arrows indicate threading dislocations and stacking faults, black arrows - Gd_2O_3 particles

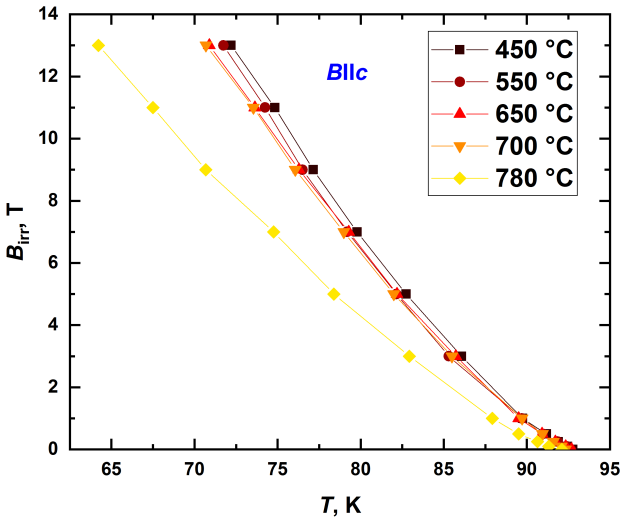

Figure 3: Irreversibility lines of pristine GdBCO films annealed at 450 °C-780 °C and t_{hold} = 10-30 min.

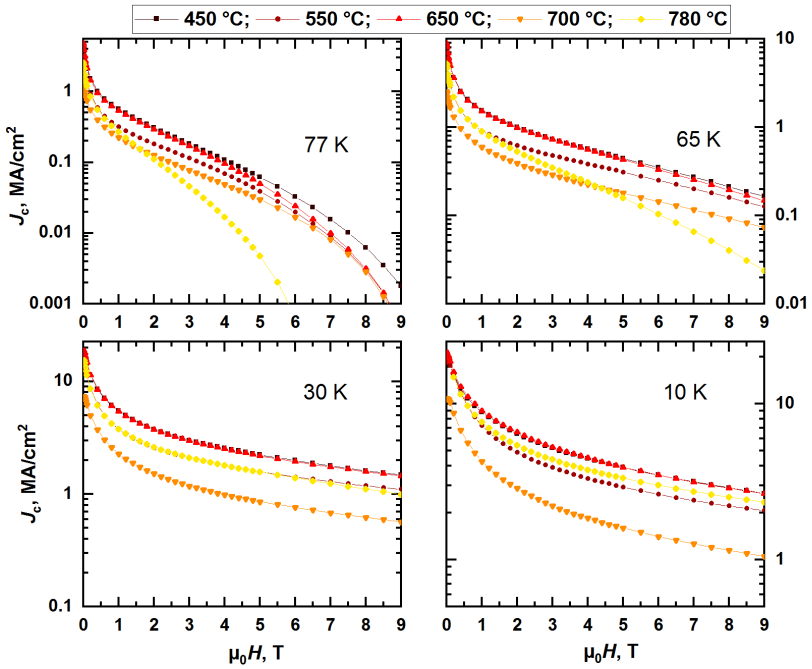

Figure 4: Field dependence of critical current density, J_c, for pristine GdBCO films annealed at 450 °C-780 °C and t_{hold} = 10-30 min.

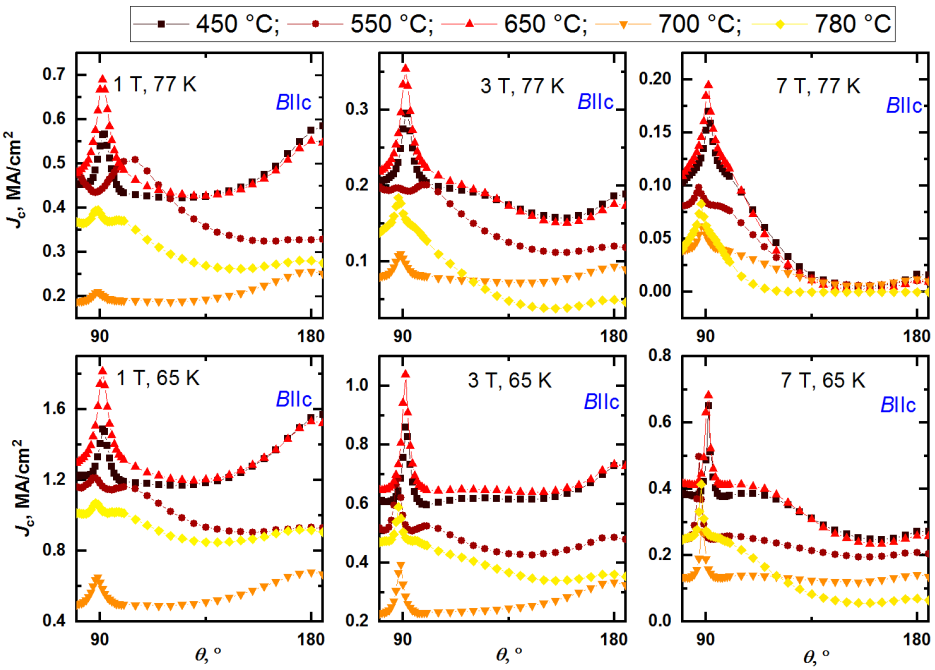

Figure 5: J_c-θ characteristics for pristine GdBCO films with T_{ann} = 450 °C-780 °C and t_{hold} = 10-30 min at 77 K (upper panels) and 65 K (lower panels) in 1, 3 and 7 T (from left to right).

T_{ann} = 780 °C, the sample with 550 °C has triangular and trapezoidally shaped Gd_2O_3 particles and ≈ 20-50 nm in size. Irreversibility lines (IL), representing transition between vortex-glass and vortex-liquid state, Fig. 3, is lowest for the sample annealed at 780 °C and t_{hold} = 10 min and the biggest shift toward high field region is achieved at T_{ann} = 450 °C, t_{hold} = 30 min.
The GdBCO films with T_{ann} = 650 °C, 550 °C and 450 °C have the highest in-field J_c values at 77 and 65 K, Fig. 4. The sample with T_{ann} = 780 °C has the strongest dependence of J_c on magnetic field. However, the situation changes at low temperatures region: the film at T_{ann} = 780 °C outperforms the films at T_{ann} = 550 °C and 700 °C but the samples at 650 °C and 450 °C still have the highest J_c in whole range of magnetic fields. The difference in $J_c(B)$ behaviour can be the result of twin boundaries and planar defects in GdBCO. At high T_{ann} = 780 °C, the diffusion rate of oxygen is higher while oxygen in GdBCO is limited due to the phase stability diagram and thus does not contribute to the formation of CuO chains but increases the stacking fault density [21]. This is in a good agreement with the calculated *c*-axis lattice parameter for GdBCO films, which is in particular directly related to the oxygen content in *RE*BCO thin films, and BF-STEM images of film microstructure. In case T_{ann} = 700 °C self-field and in-field J_c values drop at low measurement temperatures due to presence of *ab*-grains, which are known to be large in size and responsible for blocking the current.
GdBCO films are characterized by strong anisotropy regarding the field orientation $J_c(\theta)$(θ-angle between B and *c*-axis), Fig. 5. The sample annealed at high temperature shows behaviour similar to YBCO films with 2 *ab*-peaks and small peak at 180 °. A small peak in the *c*-direction appear due to threading dislocations and the small density of Gd_2O_3 nanoparticles, as it seen on Fig. 2 (A-B). At T_{ann} = 700 °C, J_c values for *ab*-peaks decrease and peak in *c*-direction appear, but the overall J_c values are the lowest due to presence of *ab*-grains. For low T_{ann} = 450 - 650 °C we observed 2 different behaviours. 1st at T_{ann} = 450 °C and 650 °C a large peak in *c*-direction appears at 1 T for 77 and 65 K. This type of behaviour was seen for GdBCO films on MgO substrate by K. Matsumoto *et al.* [6] and by W. J. Oh *et al.* [13] and was explianed as an effect of post-annealing of GdBCO CCs. This type of large peak in *c*-direction appears due to pinning on anti-phase boundaries and *a*-axis domains. At T_{ann} = 450 °C, the ratio between peak values of J_c at 180° and 90° is larger compared to T_{ann} = 650 °C, thus confirming the fact that the density of the stacking faults can be reduced by decrease of the oxygenation temperature. 2nd at T_{ann} = 550 °C for 1 T and 77 K there is flat region between 140° and 180° and additionally large peak between 90° and 120° region which further creates "volcano" in *ab*-direction. However, peak in *ab*-direction appears at higher magnetic fields. This type of behaviour at 1 T and 77 K is due to combination of planar and spherical defects in GdBCO, as it can be seen from BF-STEM images. Recently, in the studies of A. K. Jha *et al.* [22] on YBCO films with Y_2BaCuO_5 nanoparticles it was shown that the pinning potential dependence on the field orientation on planar defect has a gap at 90°, while for spherical defects it has a peak behaviour with maximum values at 90°, thus combination of these 2 types of defects gives a peak behaviour between 90° and 120°. Similar behaviour with "volcano" in *ab*-direction can be seen in the work by T. Sueyoshi *et al.* [23] for YBCO films with crossed columnar defects which can be also applied to the case of 550 °C sample due to triangular and and trapezoidal boundaries of Gd_2O_3, which have approximately 60°-120° between sides.

3.2. Influence of oxygenation in BHO nanocomposite GdBCO thin films

In our previous work on GdBCO-BHO nancomoposite films [9], we have shown that 800 °C, 10 Hz, 0.4 mbar can be considered as optimum deposition condition in our experimental set-up. Therefore, we used these conditions also for this study. Maximum self-field J_c of 2 MA/cm^2 and the maximum pinning force density of $F_{p,max}$ = 11.9 GN/m^3 at 77 K is achieved at T_{ann} = 700 °C and t_{hold} = 20 min, Table 1. It can be seen that the presence of columnar defects in GdBCO matrix decreases T_c and J_c values due to strain, which BHO nanocolumns induce and concurrent

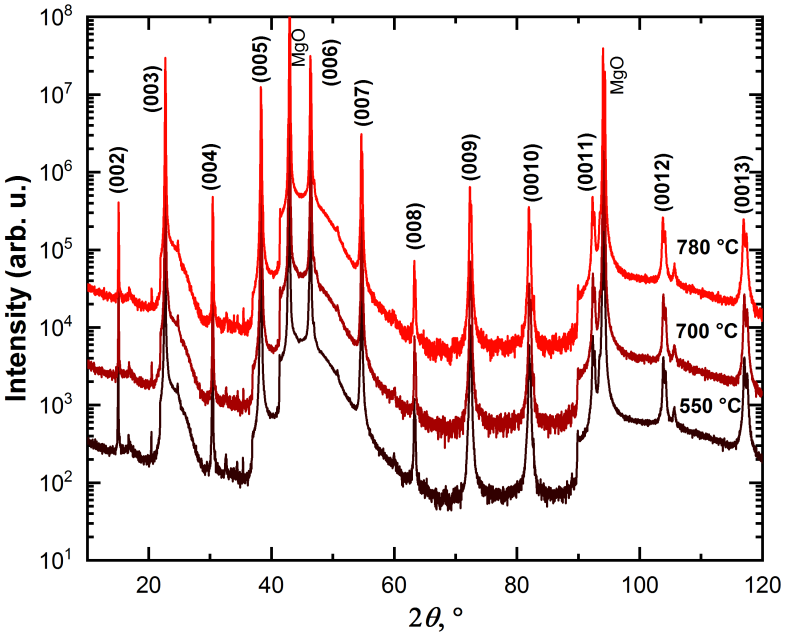

Figure 6: $\theta - 2\theta$ scan of PLD-grown GdBCO-BHO nanocomposite films on MgO substrate annealed at 550 °C-780 °C and t_{hold} = 10-30 min. All samples show GdBCO (00l) peaks. BHO peaks are not visible in XRD due to strong overlap with MgO peak.

oxygen-deficient regions surrounding BHO nanocolumns [24]. This effect of secondary phases were shown in the work of K. Ko on GdBCO films with $BaSnO_3$ on CeO_2-buffered IBAD-MgO templates [25], and similar results were achieved in our previous work on influence of T_{sub} and v_{dep} on transport properties in GdBCO+2.5wt% BHO thin films grown on $LaAlO_3$ single crystals. All samples show GdBCO (00l) peaks indicating strong c-axis orientation, Fig. 6. Regardless of BHO introduction into GdBCO matrix, additional peaks from BHO can not be seen due to strong overlap of BHO(002) peak with strong MgO (002) substrate peak. A cross-sectional BF-STEM image of the sample annealed at 700 °C shows BHO columns with diameter of ≈ 1-3 nm along the c-direction and with a splay up to 20°. The elongated growth of BHO nanocolumns appears due to low lattice mismatch between GdBCO and BHO [26]. All nanocomposite samples show the typical S-shape of the IL, Fig. 8, with matching field $B_\Phi \approx 6$ T, which is another confirmation of the nancolumn formation in the GdBCO matrix. Similar shape was shown in the references [27,28]. In contrast to pristine films in GdBCO-BHO nanocomposite the highest in-field J_{c} is achieved at higher T_{ann} = 700 °C and t_{hold} = 20 min, Fig. 9. This effect of higher oxygenation temperatures may appear due to oxygen-deficient areas around columnar defects, and higher diffusion rates may be necessary for not only the formation of the CuO chains in GdBCO, but also for regeneration of those areas. Furthermore, T_{ann} = 700 °C and t_{hold} = 20 min can be considered as an optimum oxygenation process for GdBCO+2.5wt% BHO because longer t_{hold} can possibly induce atomic diffusion at the boundaries between GdBCO and BHO, thus forming sharper and well defined interfaces and therefore lower splay, which may correspond to a clearer S-shape of IL. The maximum pinning force density $F_{\mathrm{p,max}} = 11.9\,\mathrm{GN/m^3}$ at 77 K and $65.2\,\mathrm{GN/m^3}$ at 65 K for the sample T_{ann} = 700 °C and t_{hold} = 20 min are similar to reported by P. Cayado *et al.* [29] for CSD-grown (chemical solution deposition) GdBCO+12

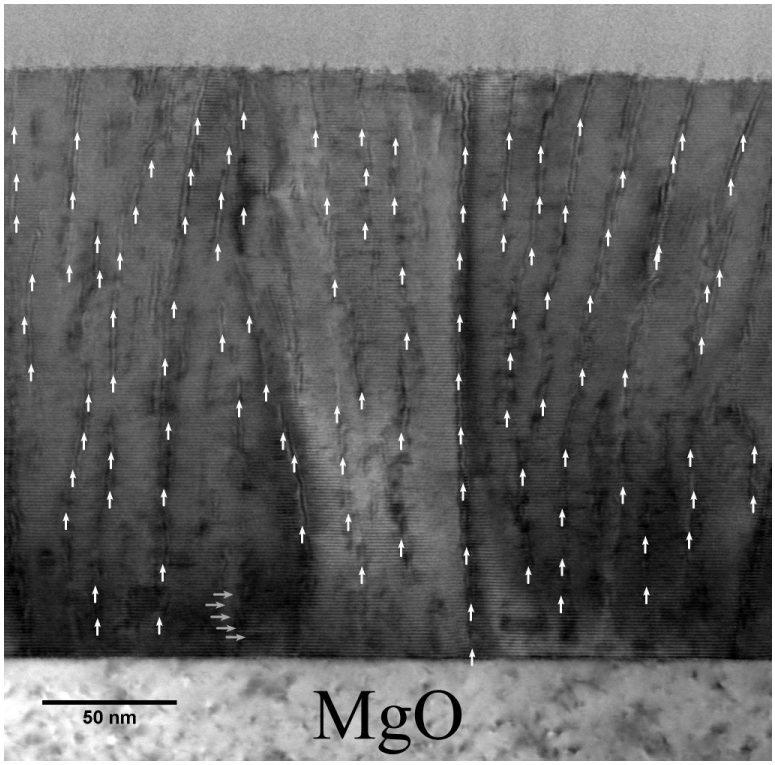

Figure 7: Cross-sectional TEM image of PLD-grown GdBCO-BHO nanocomposite film on MgO substrate annealed at 700 °C and t_{hold} = 20 min. White vertical arrows indicate BHO nanocolumns and grey horizontal arrows stacking faults.

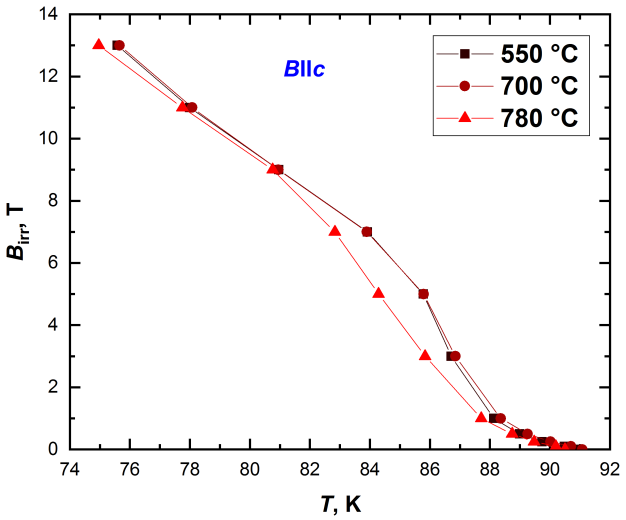

Figure 8: Comparison of ILs for GdBCO-BHO nanocomposite films annealed at 550 °C-780 °C and t_{hold} = 10-30 min.

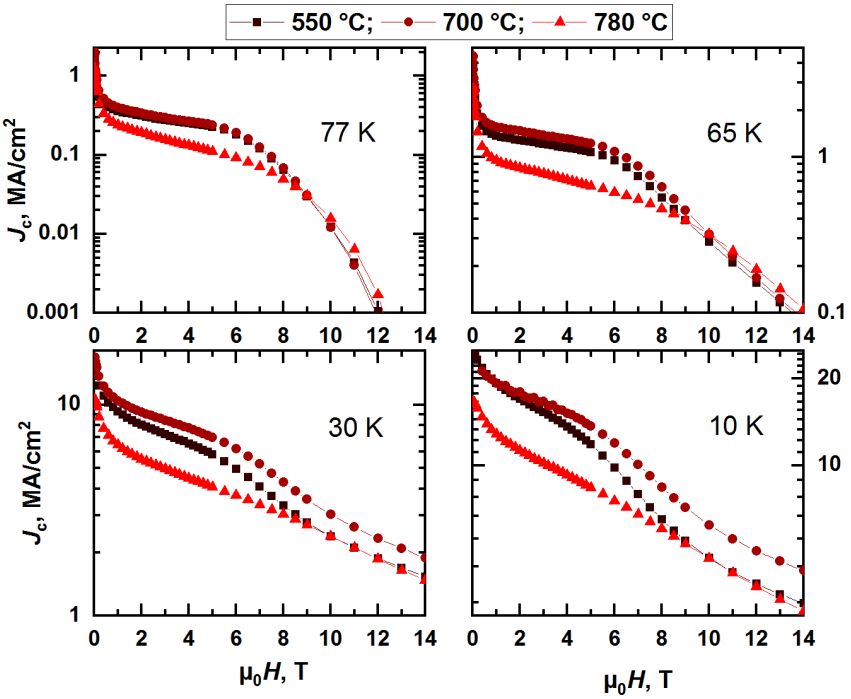

Figure 9: Field dependence of critical current density, J_c, for BHO containing GdBCO films annealed at 550 °C-780 °C and t_{hold}=10-30 min.

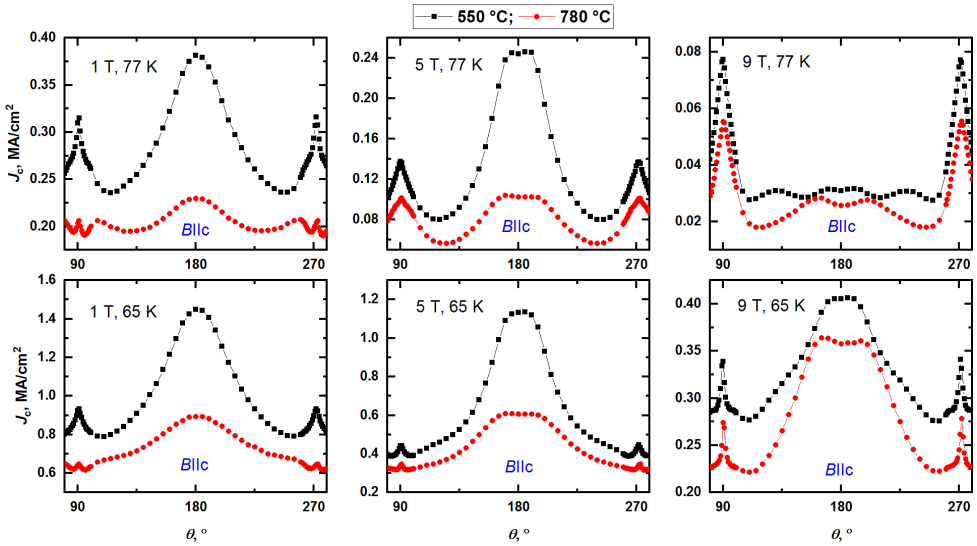

Figure 10: J_c-θ characteristics for BHO containing GdBCO films with T_{ann}=550 °C-780 °C and t_{hold}=10-30 min. Upper line represent J_c anisotropy at 77 K and 1, 5, 9 T; lower line - 65 K and 1, 5, 9 T

mol% BHO on $SrTiO_3$ single crystals, however they are 2 times lower compare to work of S. Awaji *et al.* [30] on PLD grown GdBCO+1.5 vol% BHO on tapes. Additionally, sample with $T_{\mathrm{ann}} = 700$ °C and 550 °C have similar in-field J_{c} at 77 and 65 K, but situation changes at low measurement temperatures. At 30 and 10 K in-field J_{c} for $T_{\mathrm{ann}} = 700$ °C at 4-14 T magnetic field region is higher by a factor of 2 compare to $T_{\mathrm{ann}} = 550$ °C.
To show influence of the oxygenation process on transport properties in GdBCO films with APCs, Fig. 10 compares $J_{\mathrm{c}}(\theta)$ of 2.5wt% BHO nanocomposite GdBCO films annealed at 550 °C and 780 °C. Both samples show clear peaks in *ab*-direction. Furthermore, $T_{\mathrm{ann}} = 550$ °C gives a large peak at 180 °which is present for 1 and 5 T at 77 K, as well as in all magnetic field at 65 K which indicates strong correlated pinning on BHO nanocolumns. J_{c} for $B \| c$ of the 550 °C sample are 2-3 times larger of the 780 °C sample. The 780 °C sample has 2 additional peaks in the 90°- 120°area at 1 T, 77 and 65 K which can appear due to pinning on nanoparticles as it was shown in work of A. K. Jha *et al.* [22] or splayed and inclined short nanocolumns. Comparison of J_{c} anisotropy at 2 different T_{ann} shows that change in post-annealing procedure for GdBCO films with columnar defects can not only increase J_{c} by a factor of 2 but also lead to a difference in defect morphology. Different defects may originate from increased atomic diffusion near the interfaces or in extreme cases even particle diffusion (for high T_{ann} and long t_{hold}).

4. Conclusion

Pristine GdBCO and GdBCO+2.5wt% BHO nanocomposite thin films were deposited at 800 °C, 10 Hz frequency, 0.4 mbar oxygen partial pressure and annealed at $T_{\mathrm{ann}} = 450$ °C-780 °C with $t_{\mathrm{hold}} = 10$-30 min in order to investigate influence of post-annealing process on tranport and pinning properties. In pristine GdBCO decrease of T_{ann} from 780 °C to 450 °C decreases the oxygen content from overdoped region to optimally-doped and decreases the stacking faults density and induces formation of Gd_2O_3 nanoparticles. In BHO-containing GdBCO films decrease of T_{ann} from 780 C to 550 °C increases J_{c} by a factor of 2.

5. Acknowledgments

We thank A. Marz for technical assistance as well as P. Cayado, M. Langer and S. Meyer for numerous fruitful discussions.

References

[1] MacManus-Driscoll J L, Foltyn S R, Jia Q X, Wang H, Serquis A, Civale L, Maiorov B, Hawley M E, Maley M P and Peterson D E 2004 *Nature Materials* **3** 439–443
[2] Goyal A, Kang S, Leonard K J, Martin P M, Gapud A A, Varela M, Paranthaman M, Ijaduola A O, Specht E D, Thompson J R, Christen D K, Pennycook S J and List F A 2005 *Superconductor Science and Technology* **18** 1533–1538
[3] Yamada Y, Takahashi K, Kobayashi H, Konishi M, Watanabe T, Ibi A, Muroga T, Miyata S, Kato T, Shiohara Y, Yamada Y, Takahashi K, Kobayashi H, Konishi M, Watanabe T and Ibi A 2005 *Applied Physics Letters* **87** 132502
[4] Vero J C D, Lee D, Shin H, Namuco S B, Hwang I, Sarmago R V and Song J H 2018 *Journal of Vacuum Science & Technology A* **36** 031506
[5] Feldmann D M, Ugurlu O, Maiorov B, Stan L, Holesinger T G, Civale L, Foltyn S R and Jia Q X 2007 *Applied Physics Letters* **91** 1–3
[6] Matsumoto K, Takahara D, Horide T, Ichinose A, Horii S, Yoshida Y, Mukaida M and Osamura K 2005 *IEEE Transactions on Applied Superconductivity* **15** 2719–2722
[7] Maiorov B, Baily S A, Zhou H, Ugurlu O, Kennison J A, Dowden P C, Holesinger T G, Foltyn S R and Civale L 2009 *Nature Materials* **8** 398–404
[8] Matsumoto K, Nishihara M and Kimoto T 2017 *Superconductor Science and Technology* **30** 104006
[9] Popov R, Erbe M, Hänisch J and Bernhard H 2019 *IEEE Transactions on Applied Superconductivity* **29** 8001005
[10] Cava R J, Hewat A W, Hewat E A, Batlogg B, Marezio M, Rabe K M, Krajewski J J, Jr W F P and L W Rupp Jr 1990 *Physica C* **165** 419–433

[11] Bennemann K H and Ketterson J 2008 *Superconductivity* (Berlin: Springer)
[12] Lee J W, Choi S M, Oh W J, Lee J H, Moon S H and Yoo S I 2016 *IEEE Transactions on Applied Superconductivity* **26** 8001906
[13] Oh W J, Park I, Lee J H, Lee H, Moon S H, Shinde K and Chung K 2018 *IEEE Transactions on Applied Superconductivity* **28** 1–5
[14] Krauns C and Krebs H U 1993 *Zeitschrift für Phzsik B* **92** 43–46
[15] Vazquez-Navarro M D, Kusumovic A and Evetts J E 1999 *Superconductor Science and Technology* **12** 1117
[16] Van Zele M, Watte J, Hasselmeyer J, Rijckaert H, Vercammen Y, Verstuyft S, Deduytsche D, Debecker D P, Poleunis C, Van Driessche I and De Buysser K 2018 *Materials* **11** 1101
[17] Kaneko T, H Toyoda, Fujita H, Oda Y, Kohara T, Ueda K, Yamada Y, Nakada I and Asayama K 1987 *Japanese Journal of Applied Physics* **26** 1956–1958
[18] Miyachi K, Sudoh K, Ichino Y, Yoshida Y and Takai Y 2003 *Physica C* **392–396** 1261–1264
[19] Takahashi K, Kobayashi H, Yamada Y, Ibi A, Fukushima H, Konishi M, Miyata S, Shiohara Y, Kato T and Hirayama T 2006 *Superconductor Science and Technology* **19** 924–929
[20] Matsushita T, Nagamizu H, Tanabe K, Kiuchi M, Otabe E S, Tobita H, Yoshizumi M, Izumi T, Shiohara Y, Yokoe D, Kato T and Hirayama T 2013 *IEEE Transactions on Applied Superconductivity* **23** 8000304–8000304
[21] Shiohara Y and Endo A 1997 *Materials Science and Engineering* **19** 1–86
[22] Jha A K, Matsumoto K, Horide T, Saini S and Mele P 2017 *Journal of Applied Physics* **122** 093905
[23] Sueyoshi T, Furuki Y and Fujiyoshi T 2018 *Superconductor Science and Technology* **31** 125002
[24] Goyal A and Wee S H 2017 *Journal of Physics: Conference serie* **871** 012039
[25] Ko K P, Choi S M, Lee J W, Ko R K, Moon S H, Park C and Yoo S I 2014 *IEEE Transactions on Applied Superconductivity* **24** 660908
[26] Shi J J and Wu J Z 2012 *Philosophical Magazine* **92** 2911–2922
[27] Horide T, Matsumoto K, Ichinose A and Mukaida M 2007 *Superconductor Science and Technology* **20** 303–306
[28] Horide T, Taguchi K, Matsumoto K, Matsukida N, Ishimaru M, Mele P and Kita R 2016 *Applied Physics Letters* **108** 082601
[29] Cayado P, Erbe M, Kauffmann-Weiss S, Bühler C, Jung A, Hänisch J and Holzapfel B 2017 *Superconductor Science and Technology* **30** 094007
[30] Awaji S, Yoshida Y, Suzuki T, Watanabe K, Hikawa K, Ichino Y and Izumi T 2015 *Applied Physics Express* **8** 023101